Short-time exposure oxidation studies on multi-component coatings and their influence on tribological behavior

Authors: B.C.N.M de Castilho[1], N. Sharifi[2], Sima A. Alidokht[1], K. Harrington[3], P. Stoyanov[4], C. Moreau[2], R.R. Chromik[1]

[1] Department of Mining and Materials Engineering, McGill University, M.H. Wong Building, 3610 University Street, Montreal, QC H3A 0C5, Canada

[2] Mechanical, Industrial and Aerospace Engineering, Concordia University, EV Building, 1515 St. Catherine W., Montreal, QC H3G 2W1

[3] Pratt & Whitney, 400 Main Street, East Hartford, CT 06118

[4] Department of Chemical and Materials Engineering, Concordia University, EV Building, 1515 St. Catherine W., Montreal, QC H3G 2W1

Abstract

NiCr-Cr_2O_3-Ag-BaF_2/CaF_2 (PS304) and NiMoAl-Cr_2O_3-Ag-BaF_2/CaF_2 (PS400) coatings provide low wear and friction throughout temperatures ranging from 25 to 700°C. However, one drawback of using NiCr as matrix component is the expansion observed in high temperatures, which can be detrimental for coating integrity in gas turbine applications. This expansion is caused by the formation of small precipitates, but the mechanisms of their formation are not fully understood since they are not observed in oxidational tests of pure NiCr. In the present study, PS304 and PS400 were sprayed by Atmospheric Plasma Spray and then heat-treated at 600°C for 1, 24, 48 and 100 hours to capture the initial moments of precipitate formation. The results have shown that the phase transformation occurring upon heat treatment is more complex than what is proposed in

literature. Experimental evidence has shown that the precipitates are formed by fluorine that diffuses from the fluorides to the NiCr driven by the oxidation of the fluorides, which form $BaCrO_4$ and $CaCrO_4$. Wear and friction, however, show minor sensitivity to this reaction, at least under room temperature test conditions. Furthermore, PS400 coatings showed lower wear when compared to PS304, with negligible expansion and no significant change in microstructure upon heat treating, indicating superior thermal stability and wear resistance under the tested conditions.

Keywords: multicomponent coatings, oxidation, heat treatment, fluorides, sliding wear

1 . Introduction

The strategy of combining multiple materials in a single coating was adopted by Sliney *et al.*[1] in the late 70's, resulting in the PS100 (NiCr-CaF_2-SiO_2-BaO-CaO-K_2O) and in a family of self-lubricating coatings for high temperature applications. These are usually produced by plasma spray, which allows the melting of all the different components due to the high energy input during the spray process[2]. In their composition, solid lubricants such as barium and calcium fluorides and silver are commonly found, especially in later developments. Meanwhile, a ceramic reinforcement (Cr_3C_2 or Cr_2O_3) is also used, to reinforce the metallic matrix, usually a nickel-based alloy.

Two of the latest developments of this family, namely PS304 (NiCr-Cr_2O_3-Ag-BaF_2/CaF_2)[3] and PS400 (NiMoAl-Cr_2O_3-Ag-BaF_2/CaF_2)[4] have been used in several industrial high temperature applications, such as thrust washer[5, 6], lift valves[7] and foil bearings[8, 9]. PS304 coatings have been applied on steam turbine components[7] and showed reduction in galling damage, even after 8500 hours operating at 540°C. Upon Energy Dispersive Spectroscopy (EDS) analysis, a glaze layer

comprised of the solid lubricants was observed on top of the coating, and a transfer film on the counterface was observed which was mainly composed of silver and chromium oxide[7].

In another study[8], a PS304 coated journal was tested against a X-750 foil bearing, in temperatures ranging from 25°C to 650°C, and friction coefficients of 0.4 were found up to 530°C, which reduced to 0.33 at 650°C. Lower wear on the coated part and on the counterface was found with increasing temperature, from 0.0046cm on the foil and 0.0025cm on the journal at room temperature to 0.0005cm for temperatures above 204°C[8]. The mechanism of wear also changed with temperature; while at room temperature no transfer film was formed, at 204°C an iron oxide layer was found covering the wear region, and for temperatures higher than 427°C, a transfer film composed of solid lubricants was observed, which indicates their active role to reduce friction[8].

Although widely used, PS304 coatings expand when exposed to high temperatures due to the formation of precipitates/voids in the NiCr matrix[10] and various attempts were made in order to explain this phenomenon. A study by Dellacorte *et al.*[10] hypothesized the formation of a chromium-rich second phase, or a chromium silicide. Ari Gur *et al.*[11] used X-ray diffraction to correlate the precipitates with the formation of chromium silicide ($CrSi_2$) after heat treat-treatment. The silicon, in this case, could have come from the processing of NiCr powder and could have reacted forming the precipitates[11].

Another explanation is given in the study by Dellacorte[12] which shows that the precipitate formation is related to the presence of fluorides near the NiCr matrix[12]. Stanford *et al.*[13] tested different compositions, with different combinations of fluorides, silver and chromium oxide and showed that only when the fluoride component was present, the precipitates were formed[13].

However, Stanford *et al.* conclude that void formation due to Kirkendall effect is the main cause of the expansion[13].

Stanford[14] proposes yet another explanation by spraying and heat treating PS304 and other two variations, one rich in chromium (Ni-30%Cr) and other poor (Ni-10%Cr). Upon more than one thousand hours of heat treatment, X-ray diffraction detected the combination of barium and calcium chromates, nickel oxide and the original components in some of the variations, and the author concludes that the precipitates are likely formed by oxides of nickel (NiO), chromium (Cr_2O_3) or a mixture of both ($NiCr_2O_4$)[14].

The PS400 composition, however, was designed to fix the issue on the PS304 coating. Thus, the matrix was changed from the NiCr to NiMoAl, and the amount of solid lubricants was reduced by half to reduce as-sprayed roughness[4].

It was shown that coatings produced with PS400 outperformed PS304 coatings, especially in temperatures above room temperature[4]. When tested in a pin on disk configuration against X750 pins and with temperatures above 500°C, PS400 showed reduced friction (0.16 at 500°C and 0.21 at 650°C) when compared to PS304 (0.25 at 500°C and 0.23 at 650°C), with more than 10-fold reduction in wear of the pin at 500°C, and more than 10-fold reduction of wear on the disk at 650°C[4].

Since there is no consensus on how these voids/precipitates are formed on PS304, the objective of this current study is to perform heat treatments at 600°C in both PS304 and PS400, focusing on low exposure times (between 1hour and 100hours) to capture the earlier stages of their formation and to propose an explanation for this phenomenon. Furthermore, since it is not clear if and how these voids/precipitates affect the wear behavior of the coatings, a few conditions were selected to

perform wear tests and to determine if these microstructural changes are detrimental or beneficial for the wear performance and to analyze the effects of heat treatment on the PS400.

2. Methodology

Coatings were sprayed on 25x25x5mm steel substrates by Atmospheric Plasma Spray (APS) with two different powder feedstocks: PS304 and PS400 (Table 1, provided by the manufacturer) acquired from Advanced Material (USA), and the spray conditions are described in Table 2. After spraying, one sample of each coating was cross-sectioned and prepared by using standard metallographic procedures. These were followed by a final step using colloidal silica (0.05μm) in a vibratory polisher Vibromet (Buehler, Germany) for Scanning Electron Microscopy (SEM) observation. After polishing, the samples were cleaned with water and soap, followed by acetone to remove any residues of colloidal silica, and then dried with hot air. Measurements of thickness were also made by SEM, in which at least three different images across the cross-section were made and 10 measurements in each picture were performed and averaged. A SU3500 (Hitachi, Japan) equipped with an Energy Dispersive Spectroscopy (EDS) detector (Oxford, UK) was used for all SEM images. For wear track images, because of charging effects, an Ultra Variable-Pressure Detector (UVD) was used in the same SU3500 microscope.

Table 1 – Composition (wt%) of PS304 and PS400

Composition (wt%)	PS304	PS400
80Ni20Cr	60	0
Ni5.5Al5Mo (METCO 447)	0	70
Cr_2O_3	20	20
Ag	10	5
BaF_2/CaF_2 eutectic (62-38%)	10	5

Table 2 – Deposition parameters used to spray the coatings by APS.

Parameters	Values
Current (A)	650
Voltage (V)	40.1
Power (kW)	26.1
Primary Gas Type	Ar
Primary gas flow rate (slpm)	35
Secondary gas type	He
Secondary gas flow rate (slpm)	35
Feed rate (g/min)	18.6

Smaller samples were cut from the original coupons and exposed to heat-treatments for 1, 24, 48 and 100 hours at 600°C and mounted for cross-sectional observation following same procedures as as-sprayed samples. The choice of temperature was based on previous literature[14] which has shown that the feature of interest could be formed in temperatures higher than 500°C and up to 800°C. However, since the idea was to capture early stages of formation of these features, a temperature inside this range was chosen.

Two exposure times at 600°C (50 and 100 hours) were selected to heat-treat the samples of both materials for wear testing. Furthermore, one as-sprayed sample of each material was tested for comparison. The surface of the samples for wear tests were ground from 600 up to 4000 grit and were also polished following the same steps as the cross-sections, including the final step in vibratory polisher. Cleaning steps were the same to the ones described for cross-sectional observation. Vickers microhardness tests (Clark Microhardness Tester, USA) were performed at the cross-section in 10 different locations at the cross-section for each coating using a load of 25gf.

Reciprocating wear measurements were performed in a TRB (Anton Paar, Austria) using a load of 5N, a frequency of 1Hz, a track length of 10mm for a total of 100m (5000 cycles) and running against 6.35mm-diameter alumina ball (McMaster-Carr, USA) at room temperature. Under these conditions, the average Hertzian contact stress was calculated at 861MPa for PS304 and 845MPa for PS400. For this calculation, only the elastic moduli of matrix components of each coating were considered, but it is expected that the real contact stress will be smaller than that due to coating defects and the presence of more compliant components in the composite coating. Nevertheless, due to the heterogeneity of the coating, the local contact stress can change significantly depending on the testing location.

A total of three wear tests were performed for each sample. The friction coefficient was automatically recorded by the tribometer, but the wear tracks and the wear on the alumina counterfaces were measured using NewView light profilometer (Zygo Corporation, USA). All wear tracks were scanned and a total of 30 cross-sectional profiles were made and averaged to calculate the total worn volume, which then was normalized by the total distance and the applied load. The same profilometer was used to measure the roughness of the samples in an area of 335x335μm at random locations in each sample.

Raman analysis was performed by using an InVia spectrometer (Renishaw, UK) with an Ar+ ion (λ=514.5nm) laser source in worn and unworn regions of the coatings subjected to wear tests and the spectra were indexed by comparing with literature data.

3. Results

3.1 Powder and as-sprayed coating characterization

The PS304 and PS400 powders are provided as a mechanically mixed powder, meaning that there is no initial bonding between the different components, as can be observed in Figure 1. In Figure 1(A), all the components of PS304 are highlighted, meanwhile on Figure 1(B), only the components of PS400 that are not present on PS304 are highlighted. The only observable change is the substitution of NiCr (light gray) for the NiAlMo (dark contrast), which consists of a Ni core surrounded by a layer of mechanically clad Mo and Al. The chemical composition of the individual powders was confirmed by EDS analysis. For both PS304 and PS400 there is a wide particle size distribution, with some particles ranging from 100μm to some in the range of 1-10μm. PS304 has a D50 of 29.4μm and the PS400 is 28.1μm and the former also show a wider distribution when compared to PS400, which could be caused by the bigger NiCr particles when compared to the NiAlMo on PS400 but could also be caused by the comminution of the brittle eutectic fluoride during mixing, generating the small particles which can be observed in Figure 1(A).

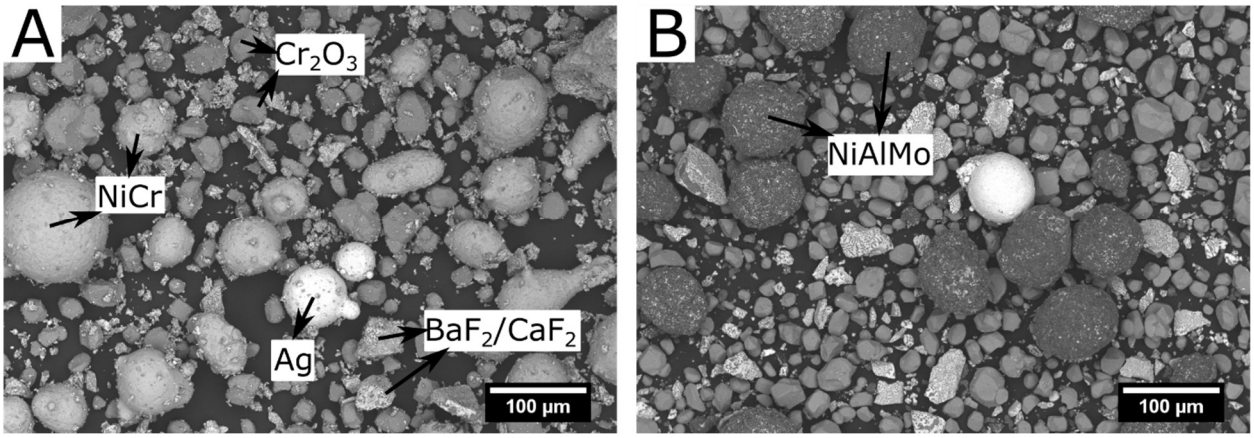

Figure 1 – Backscattered Electron (BSE) image of feedstock powder: (A) PS304 and (B) PS400

Upon spraying, a 320±19µm coating was produced with PS304 powder and a 286±11µm coating with the PS400, as shown in Figure 2, in which ± represents the standard deviation. The as-spray roughness was similar for both coatings, with both showing R_a close to 13µm. However, upon polishing the samples before wear testing, it was reduced to below 1µm.

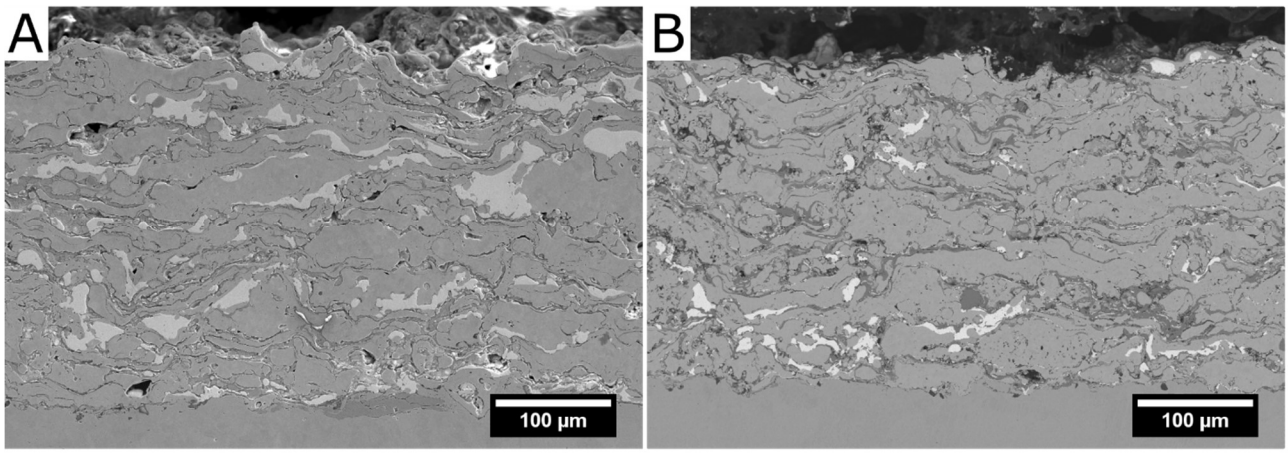

Figure 2 – BSE image of as-sprayed coatings: (A) PS304 and (B) PS400

3.2 Heat treatment effects on microstructure, morphology, and mechanical properties

The cross-sections of the PS304 coatings treated at 600°C for 1 and 100 hours are presented in Figure 3(A) and (B). In the regions marked in blue, the formation of the features of interest is

highlighted, which are present close to NiCr splat boundaries close to BaF_2/CaF_2 particles. This corroborates the results found by DellaCorte[12] and Stanford *et al.*[13] which observed that the features only appeared in samples which had the eutectic fluorides in their composition.

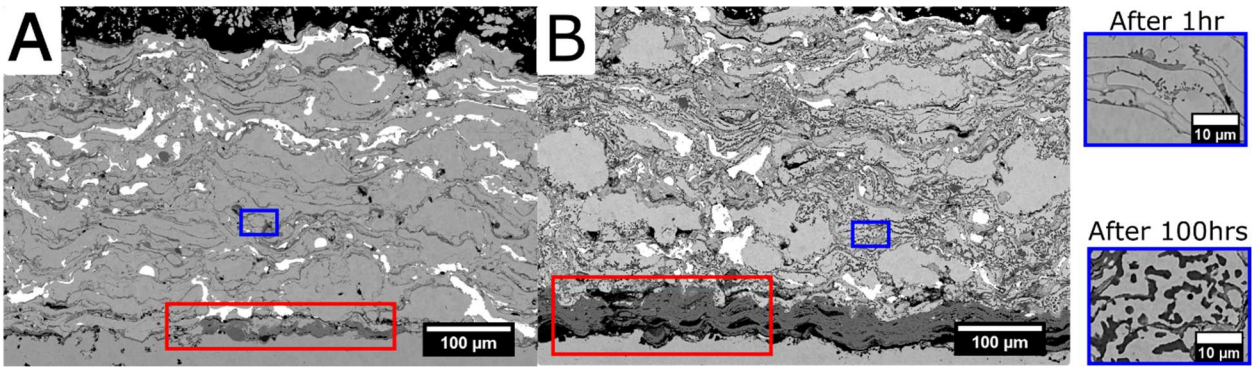

Figure 3 – BSE images of heat-treated samples at 600°C: (A) after 1 hour, (B) after 100 hours and detailed images of precipitates. Red highlights oxidation of steel at coating-substrate interface. Blue marked regions are shown at higher magnification

Also, in Figure 3(B), the 100 hours heat treatment resulted in the formation of an oxide layer at the coating-substrate interface. EDS analysis of the region marked in red showed oxygen and iron.

Samples treated at 600°C showed particular microstructural modifications showed in Figure 4. In these regions, EDS revealed strong signals of fluorine and chromium indicating that in fact these are precipitates, which are mainly composed of F and Cr, likely CrF_2 or CrF_3. Their formation can be related to some studies[15-17] which used first-principles simulation to understand the adsorption and diffusion of fluorine at the surface of Ni and NiCr. To simulate the presence of chromium, one atom of Cr was added by substituting one Ni atom and in their findings, it was shown that the Cr-F bonding is stronger than Ni-F[15].

Although no other report was found of fluorine diffusion in solid state, there are reports of similar phenomenon when Ni-based alloys containing chromium are exposed to molten fluoride salts. In a study comparing Ni-based alloys with chromium in their composition, it was shown that

chromium is depleted during exposure at high temperatures[18]. Furthermore, the more chromium an alloy has, the more it is corroded by fluorine presence and more chromium is present in the salt after the test, indicating that the byproduct of the reaction is removed by the liquid salts[18].

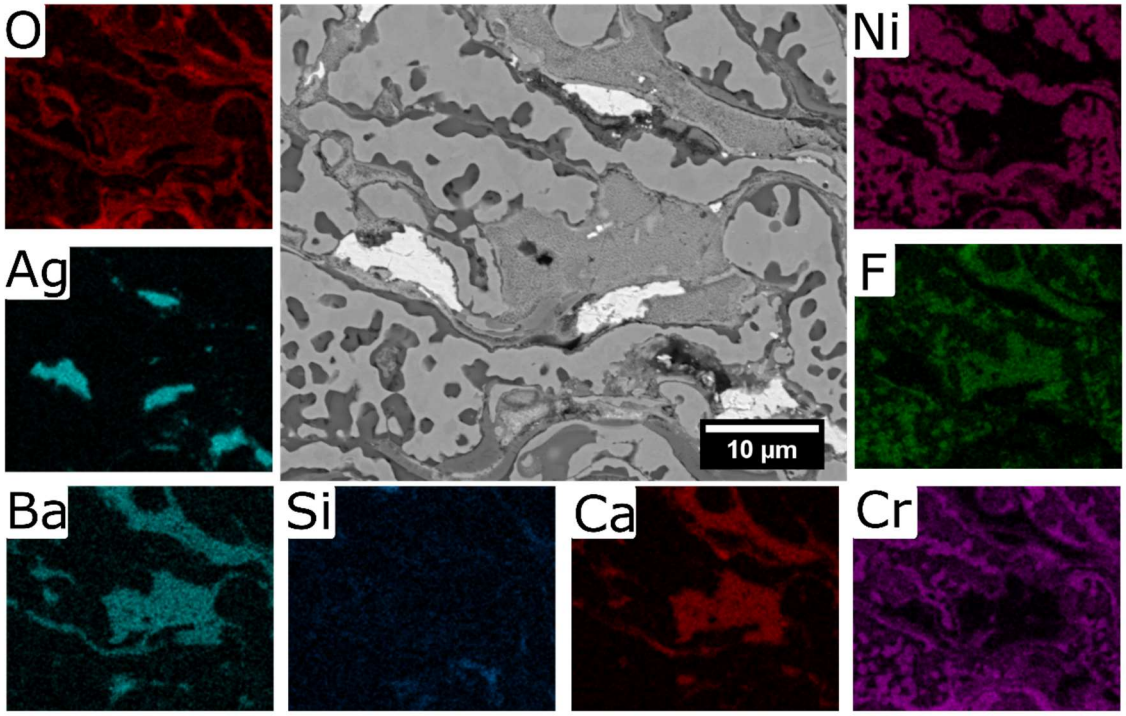

Figure 4 - EDS mapping of PS304 at 600°C, after 24 hours

In the PS304 coatings, however, due to the constraints imposed by splat boundaries and the presence of other materials such as silver and chromium oxides, the fluorine diffuses inside the NiCr splats forming the chromium fluorides, which has lower density and then they start growing, causing the expansion of the coatings.

In Figure 5, on regions marked as A and B, the EDS analysis confirms that the main composition of the precipitates is chromium and fluorine, indicating the same composition as observed on the precipitates of Figure 4. In region C, a strong signal of barium is found, combined with oxygen. This could indicate the formation of BaO, but the presence of chromium in the same region also

suggests that some $BaCrO_4$ was formed. The oxidation of pure barium fluoride and calcium fluoride occurs by releasing F^{-1} ions, which are replaced by the oxygen, in temperatures as low as 600°C for BaF_2 [19] and 800°C for CaF_2 [20].

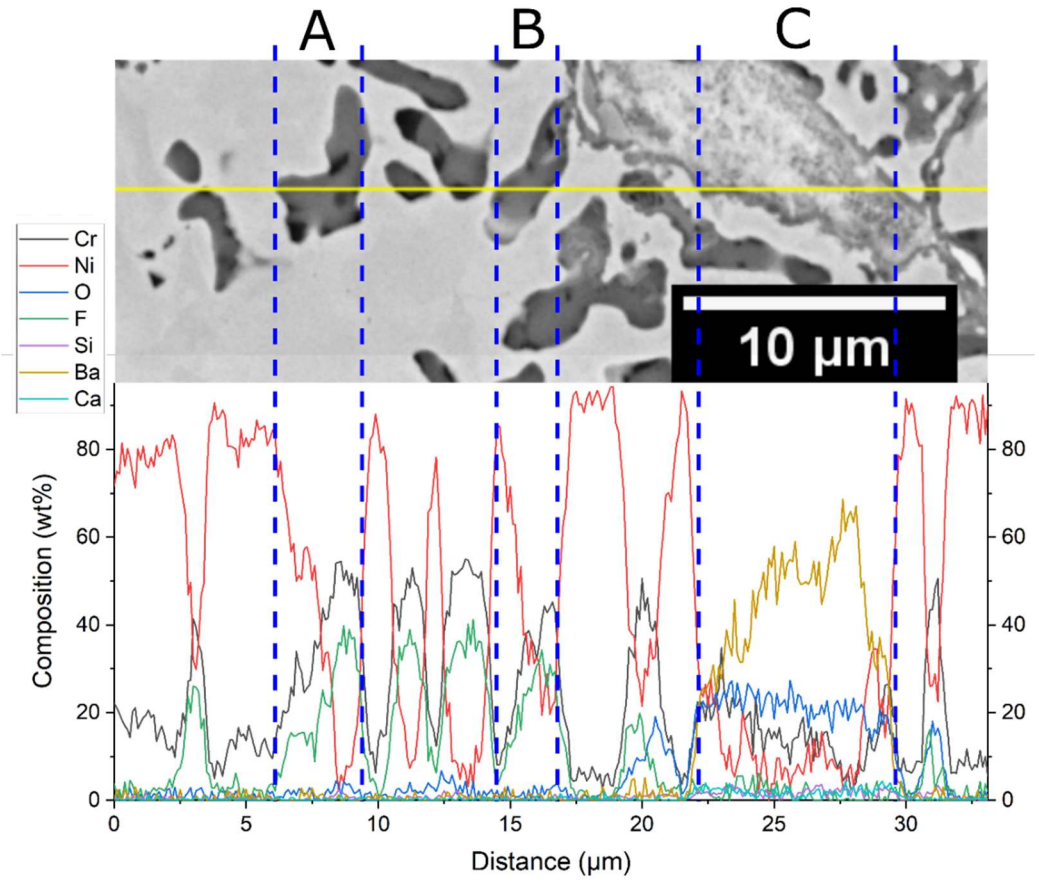

Figure 5 – Linescan using 15keV and spacing of 0.1µm between points showing the presence of fluorine on the precipitates and the depletion of fluorine on the original eutectic

The heat treatment on PS400 coating formed no precipitates regardless of the exposure time, as can be observed in Figure 6. Differently from PS304, the PS400 coatings does not have metallic chromium in the composition of the matrix, which is composed of pure nickel encapsulated by a layer of molybdenum and aluminum. The presence of chromium is limited to the chromium oxide component, which is sprayed in the mixture, and no evidence of migration of fluorine was observed

towards the chromium oxides, neither for PS304 nor for PS400, thus not forming the chromium fluoride components on the PS400 coating. Furthermore, chromium oxide is more stable than the metallic chromium in the matrix of PS304, which makes it more susceptible to the fluorine attack.

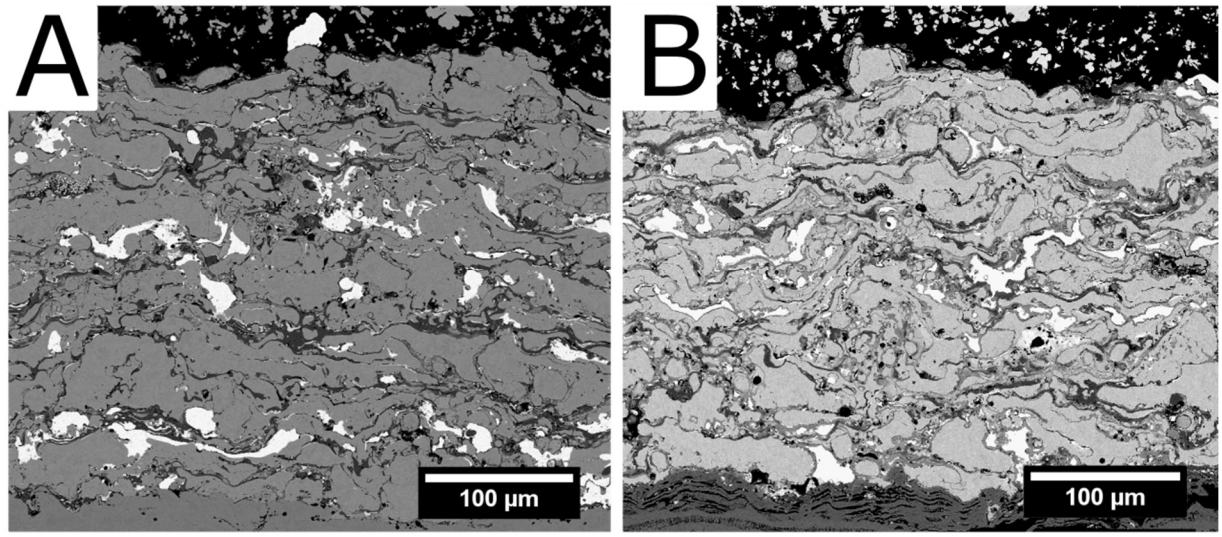

Figure 6 - Cross-section backscattered image of PS400: (A) as-sprayed and (B) after 100 hours at 600°C with minimal microstructural change

Vickers hardness testing was used to probe the cross-sections and to identify if the heat treatment had any effect on hardness for both PS304 and PS400, as shown in Figure 7. Both coatings showed an increase in hardness after heat treated at 600°C, however both reached a plateau after 24 hours of treatment. When combining the hardness measurements with the indent observation by optical microscopy (Figure 8), the results indicate that the effects of diffusion improved the bonding of the splats due to the heat treatment, increasing the cohesive strength. PS400 continued to have lower hardness than PS304 throughout the whole heat treatment, most likely due to the matrix consisting of pure Ni in the former and NiCr on the latter. Both PS304 and PS400 showed increase in hardness and a plateau after the same time, which favors the explanation of an increase in

hardness due to better bonding, and increase in cohesion due to inter-splat diffusion, especially between metallic components, and not due to the precipitates being formed in the NiCr matrix.

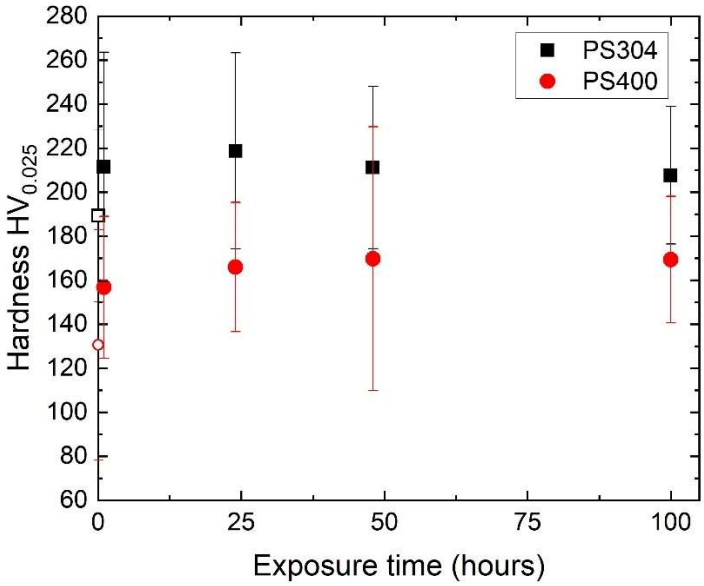

Figure 7 – Vickers micro-hardness of PS304 and PS400 coatings with standard deviation plotted versus exposure time at 600°C, the unfilled symbols represent as-sprayed hardness

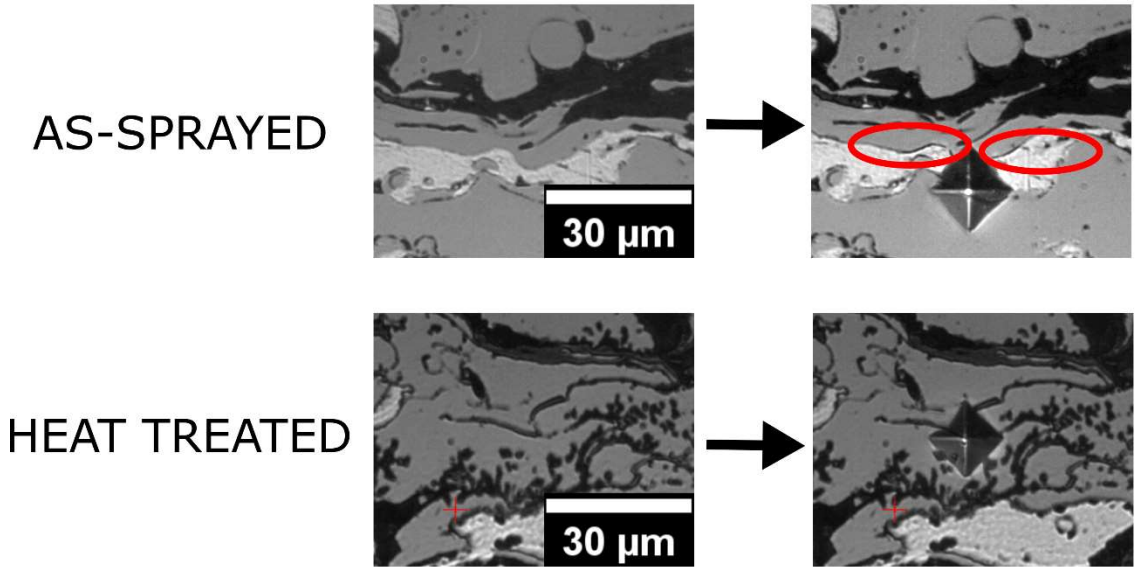

Figure 8 - Optical image of indents on as-sprayed and heat treated (100 hrs at 600°C) PS304 samples. The red marks indicate debonding between splats due to hardness testing

As a result of the formation of the PS304 precipitates, the increase in thickness as a function of exposure time is presented in Figure 9, in which PS304 showed a continuous expansion from 1 to 100hrs. On the other hand, the PS400 coatings show barely any expansion even after 100 hours at 600°C. To analyze just the effects produced by the precipitate formation on PS304, the wear tests were performed after removing the oxide layer on top of PS304 and PS400 by grinding and polishing the surface.

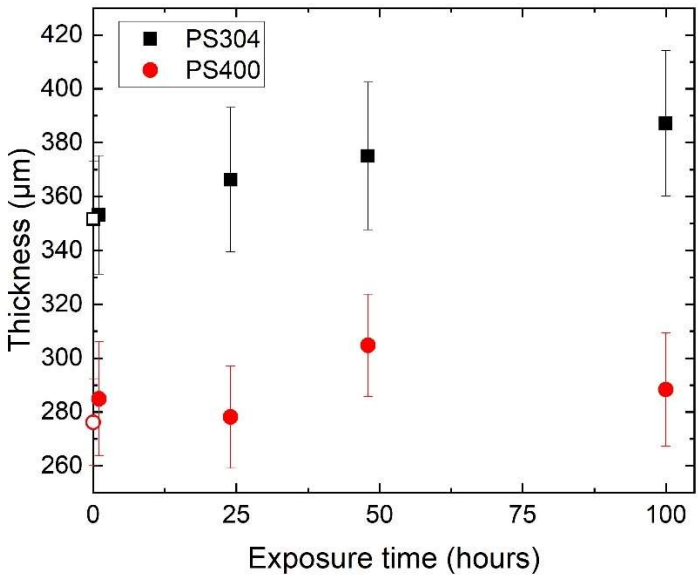

Figure 9 - Increase in thickness for PS304 and PS400 with standard deviation as a function exposure time at 600°C, the unfilled symbols represent as-sprayed thickness

3.3 Wear results

3.3.1 - Friction

Friction coefficient curves of as sprayed and heat-treated samples are shown in Figure 10. In the PS304 coatings (Figure 10(A)), a peak in friction coefficient is observed after approximately 800 cycles for heat-treated samples and this peak is only observed after 1200 cycles in the as-sprayed sample. Following this peak, the friction coefficient decreases and get stable between 0.6-0.65 for

samples that were heat treated. For as-sprayed samples, the trend of increasing friction coefficient is observed up to the end of the test. On the other hand, for PS400 coatings (Figure 10(B)), the heat treatment had no effect on friction coefficient, and the results show a stable growth during running in period, followed by stabilization of friction after 2500 cycles.

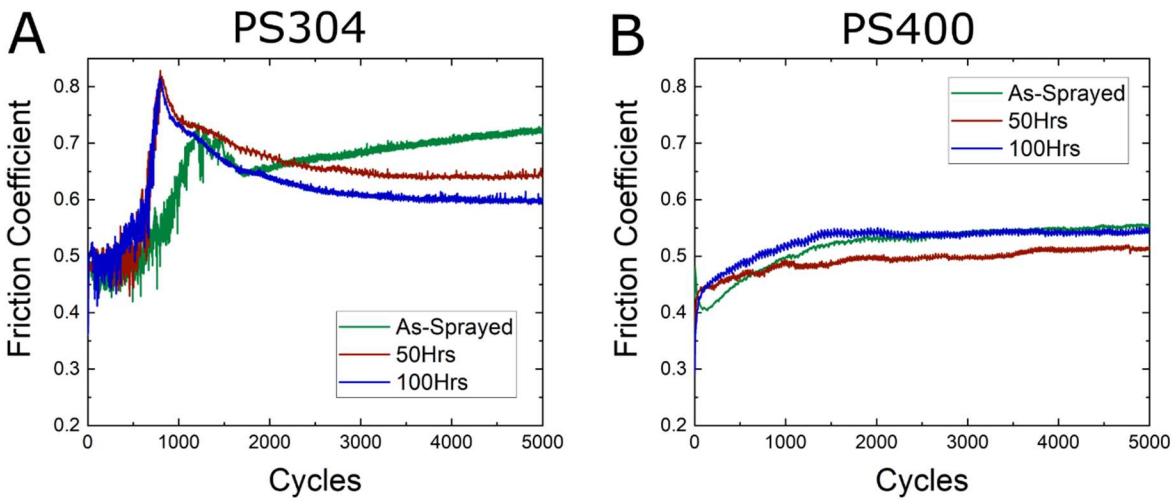

Figure 10 - Friction curves for PS304 and PS400 tested at room temperature as a function of number of cycles and heat treatment duration at 600°C

To further understand the mechanisms of friction and wear in the PS304 samples, i.e. why there was a peak of friction, two tests were performed on the sample heat treated for 50 hours and then interrupted after 500 and 1000 cycles. The interrupted test showed the same behavior of the full curve, consisting of a peak at around 800 (not shown).

3.3.2 - Wear

In Figure 11(A), the wear rates on all samples are represented, and in detail, Figure 11(B) shows the results for the PS400. For all PS304 samples no visible trend in wear can be determined, meaning that the wear behavior of the samples is not influenced by the heat treatment nor by the

presence of the precipitates. Furthermore, Student's t-test has shown that the wear rates for PS304 are statistically the same. The non-homogeneity of such multicomponent coating increases the dispersion of the wear measurements, which means that depending on the tested region, the lack or abundance of soft metal and brittle phases may change the wear behavior. This leads to the increase of the error bar for all samples (PS304 and PS400).

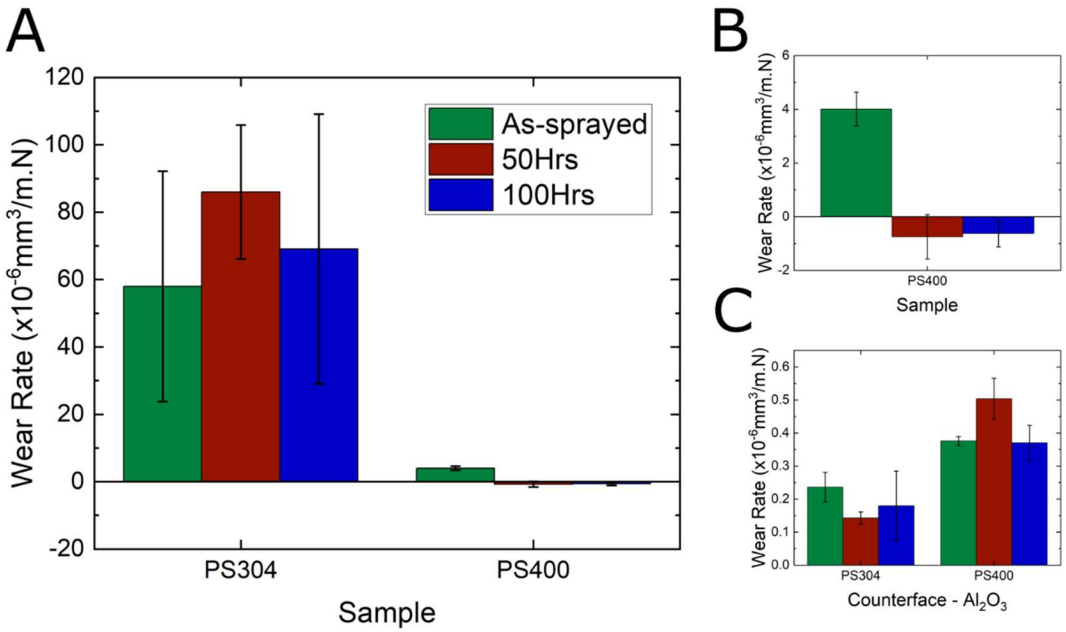

Figure 11 - Wear rate with standard deviation: (A) as a function of heat treatment duration at 600°C, (B) detailed graph for PS400, (C) at the counterfaces

For the PS400 samples, a change in the wear behavior can be observed, moving from a positive wear (here considered as the sample being worn out) to a negative wear (material is being transferred from the counterface to the sample). One possible explanation for such change in trend is the improved bonding between the particles achieved by the heat treatment. Nevertheless, for as-sprayed and heat-treated samples, PS400 showed reduced wear when compared with PS304 (more than one order of magnitude smaller).

The wear rate measurements in the counterface are presented in Figure 11(C), in which a reduced amount of wear in the order of 10^{-7} is observable for all samples. However, the lower wear observed for the PS400 samples comes at the expense of higher wear on the counterfaces, which was between two and three times higher when compared to the PS304.

The wear rates and removed volume of the interrupted test for the PS304 are shown in Figure 12, as a function of the total number of cycles. The removed volume increases with the number of cycles, which is expected. However, it increases in a non-linear way. The wear rate is smaller after 5000 cycles than after 500 and 1000 even though the data was cumulative (the wear rate showed in Figure 12 considers the full 5000 cycles) which means that most of the wear occurred during the earlier stages of testing. When considering only the volume lost during the last 4000 cycles, the wear rate is even smaller than showed in the figure, around 2.1×10^{-5} $mm^3/m.N$.

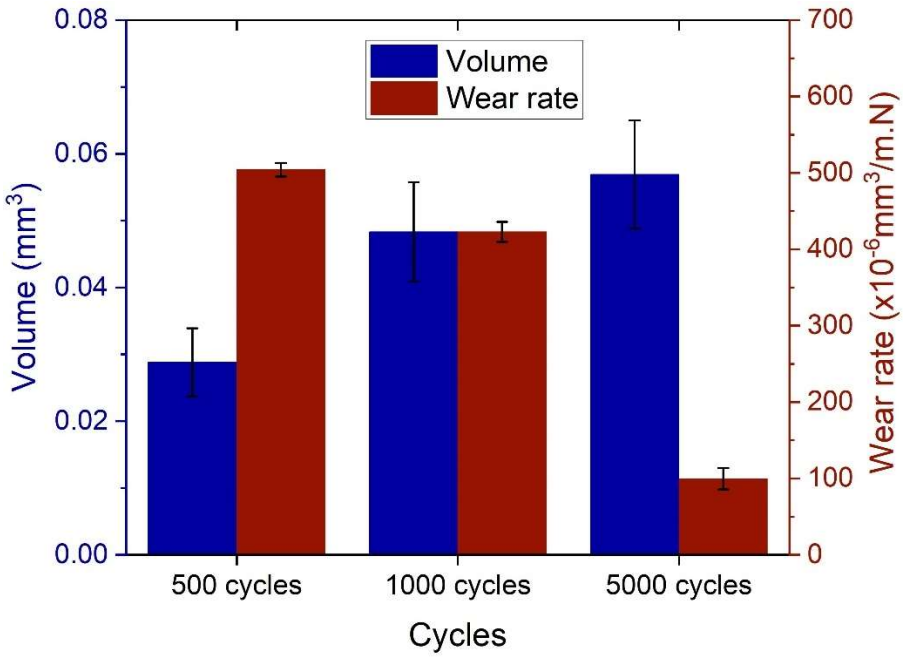

Figure 12 - Interrupted wear test and measurements of wear rate and removed volume with standard deviation of PS304 heat-treated for 50 hours at 600°C

3.3.3 – Raman analysis

The Raman spectra were collected in multiple regions of the wear track but those showing no signal (indicating metallic regions) were omitted. Furthermore, when multiple regions showed spectra with the same peaks, only one was represented in the plot. For the PS304 tested as-sprayed, showed in Figure 13(A) peaks related to NiO [21] and Cr_2O_3 [21, 22] were found at the wear track, but also a convoluted peak at 777cm^{-1} and 808cm^{-1} indicate the formation of $AgCr_2O_4$ [23] in the wear region. The peak at 856cm^{-1} could be attributed to chromium oxides of the type CrO_2, CrO_3 or Cr_8O_{21} [22]. When investigating the wear track of PS304 after 100 hours heat treatment (Figure 13(B)), different peaks are observed, which could be traced to the formation of $BaCrO_4$[24], $CaCrO_4$[25], and $NiCr_2O_4$[26-28] and peaks related to bending and stretching of Cr-F bonding[29].

For the PS400, analysis on sample unworn and worn (with and without heat treatment) shows either regions with no Raman activity, likely a metallic mixture (for worn samples) or the as-spray metallic splats (unworn sample). However, it also showed the peaks in Figure 13(C) in different regions of all wear tracks and in some regions of the as-deposited sample. Those are correlated to the formation of silver molybdates [30, 31], but other types of molybdates, such as barium and calcium could also be present since the peaks for these molybdates are commonly found close to each other[32]. NiO and Cr_2O_3 were also identified in the wear track and on as-sprayed coatings, probably coming from the oxidation during spray in splat boundaries for the former, while the latter is one of the components of the coating.

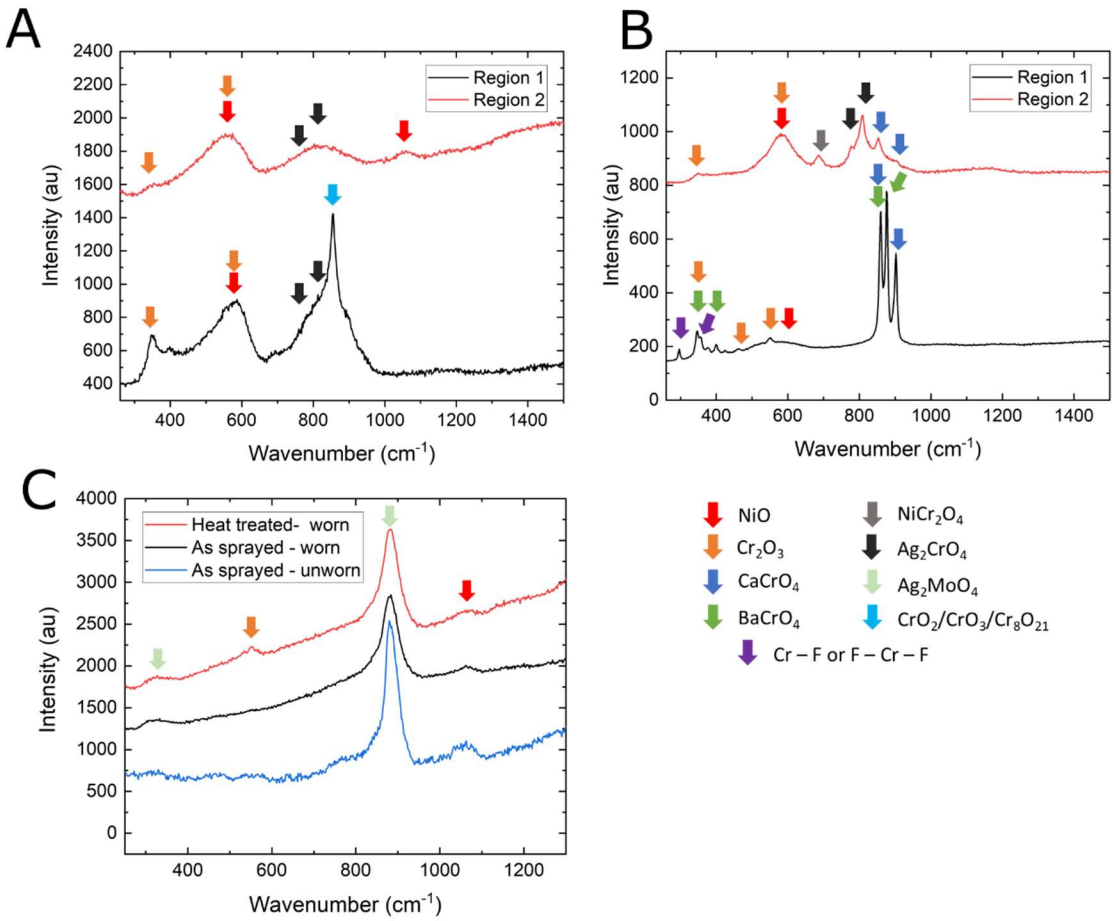

Figure 13 - Raman peaks for (A) as-sprayed PS304 tested at room temperature; (B) PS304 tested at room temperature after 100hours at 600°C, (C) PS400 unworn and worn regions (heat treated for 100hours and not heat treated)

3.3.4 – Counterface characterization

When analyzing the counterfaces in Figure 14, a common feature was the presence of grooves, indicating that, at least in later stages, abrasive wear on the counterface is occurring, especially for PS400 coatings. These grooves, which are not part of the initial morphology of the counterface, were filled with metallic material, indicating the metallic transfer from the coating to the surface of the alumina balls. EDS analysis on these particles attached to the surface shows metallic NiCr at the counterfaces tested on PS304 and metallic Ni for the PS400 regardless of heat treatment.

Furthermore, the presence of silver was found in the entire surface, in the form of small islands, shown in detail in Figure 14, indicating that adhesive wear also played a role during the wear of those coatings.

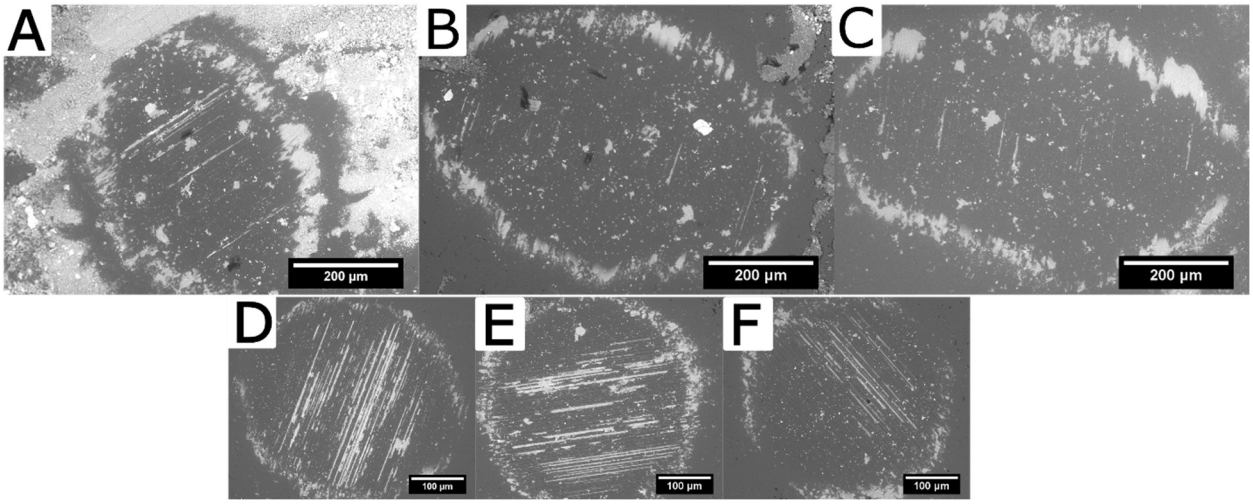

Figure 14 - SEM image of the counterfaces running against: (A) as sprayed, (B) 50 hours heat treated and (C) 100 hours heat treated - PS304 coatings and (D) as sprayed, (E) 50 hours heat treated and (F) 100 hours heat treated - PS400 coatings

The counterfaces running against PS304 showed negligible wear with shallow wear scars. However, these were spread in a bigger area than PS400 counterfaces. Since the PS304 coating had wider wear track, it makes sense to find a wider wear scar in the counterpart. This indicates that, during the test, due to the ejection of wear debris, the area in contact with the counterface increased, and a reduction on the contact pressure happened. On the other hand, for the PS400, the wear depth on the counterface was significantly higher, but the area of contact was smaller when compared to the ones that ran against PS304.

3.3.5 – Wear Mechanisms

Both PS304 and PS400 showed a tribolayer covering most of the track surface and EDS analyses indicate the presence of nickel and oxygen throughout the whole track, with oxygen reaching 25wt% in some regions inside the tracks, and with the presence of some spots with metallic material exposed, meaning that an oxide layer was formed at the wear track during testing. Cracks can be observed throughout the track surface indicating both the brittle behavior of the oxide layer combined with the effects of fatigue after 5000 cycles.

PS304

The testing on PS304 was characterized by an unstable friction period, followed by a peak in friction and then a decrease in friction values as observed in Figure 10(A). Furthermore, stabilization of the friction was observed for the heat-treated samples, which was not observed for the sample tested in the as-sprayed condition. For the latter, after the reduction in friction, the frictional values kept increasing in a constant manner. By comparing the Raman analysis on the wear track from Figure 13(A) and (B), the presence of non-stoichiometric chromium oxides was observed in the as-sprayed coating. These are likely being formed during the sliding and are constantly being mixed in the wear track. On the other hand, the as-sprayed sample did not form the plethora of ternary oxides observed for heat-treated samples, which are known to reduce friction.

For heat-treated PS304 samples, specifically the one heat treated at 600°C for 50 hours, it possible to understand the mechanisms of wear and friction by interrupting the test after 500 cycles and 1000 cycles in the sample heat treated at 600°C for 50 hours. In the earlier stages (below 800 cycles), adhesive wear seems to be the main mechanism, in which metallic components of the

PS304 get attached to the surface of alumina. These are mechanically mixed and then ejected in the form of oxide debris. Chemical analysis by EDS has shown the presence of not only Ni and Cr on those debris, but also silver, barium, and calcium, all mixed and oxidized. Some trace amounts of fluorine were also observed.

This early stage with unstable friction is also marked by smearing of silver component in the wear track (Figure 15(A)), indicating the mixing of the different components not only on the debris, but also on the wear track. Furthermore, it is likely that during this part the silver based ternary oxides are produced due to the intense mixing in the contact region combined with frictional heating up to the friction peak.

The peak of friction followed by the decrease in friction values can be correlated to the formation of the oxide layer covering the wear track. Up to this point, the contact was mainly the alumina against the fresh metal. However, after the friction peak, the wear track is mostly oxidized (Figure 15(B)), moving the contact from metal-ceramic to ceramic-ceramic, thus minimizing the adhesive component of the friction force, reducing the overall friction coefficient.

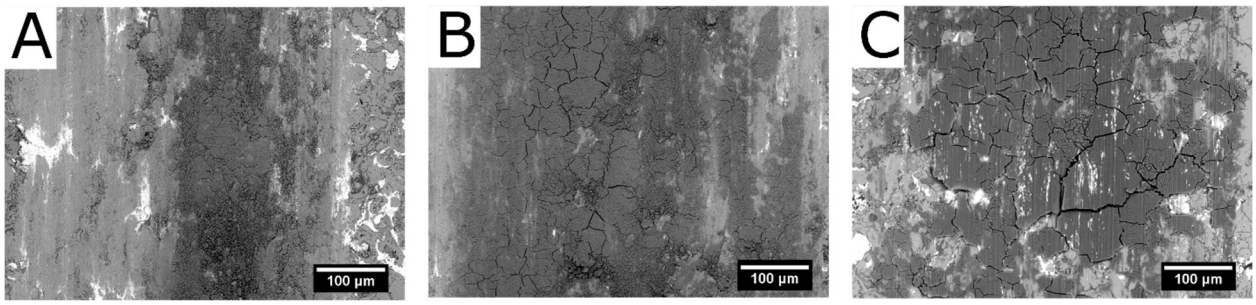

Figure 15 - Wear track evolution of PS304 (heat treated for 50 hours at 600°C) after: (A) 500 cycles; (B) 1000 cycles and (C) 5000 cycles

In Figure 15(B) an oxide layer is already covering most of the surface of the wear track, with few points of exposed metals. This surface is covered by loose debris and the wear mechanism moves

from adhesive to abrasive. After this point up to the end of the test (Figure 15(C)), the oxide layer formed at the surface, brittle in nature (confirmed by the cracking throughout the whole tribofilm), starts to gets polished by the small debris particles, but further wear keeps happening by the detachment of the tribolayer, exposure of fresh metal and further oxidation, although at a slower rate, as can be seen in Figure 16.

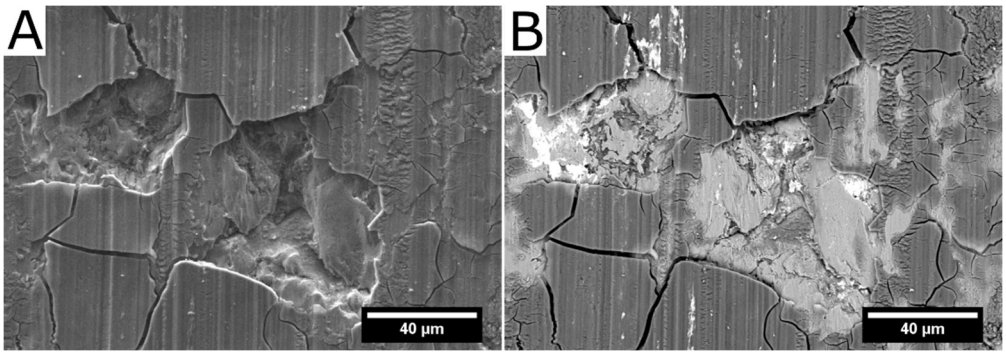

Figure 16 – UVD (A) and BSE (B) images of the wear track showing detachment of the oxide layer and the exposure of fresh metal

The presence of barium and calcium chromates on the wear track, combined with the presence barium chromate in the cross-sectioned samples confirmed by EDS, leads to the interpretation that these were formed during heat treatment and not during the wear. However, their presence on the wear track could have helped to establish the oxide layer sooner than what was observed for the as-sprayed sample.

The analysis by Raman on the wear track of the samples tested as sprayed shows the presence of NiO, Cr_2O_3 and Ag_2CrO_4. These results indicate that the early mixing (before peak) of the Ag and Cr and further oxidation might be playing an important role to reduce the friction coefficient of the coating in later stages.

Based on the wear results for all samples, it seems that, even though the oxide layer being formed at the surface is not stable, it modifies the contact region and the mechanism of wear. The contact changes from predominantly metal-ceramic in the early stages to predominantly ceramic-ceramic in later stages which reduces the amount of debris being formed and reduces the wear rates.

PS400

For the PS400, a different mechanism seems to be in place. The friction curves show a smooth run-in period, followed by stable friction coefficient throughout the whole test. The oxidation of the surface is more readily achieved, which avoids the formation of the bigger debris particles observed in the earlier stages of testing on the PS304. Instead, small debris are observed at the edges and borders of the wear tracks (Figure 17 (A)), which could have come from the wear on the counterface or by the comminution of the tribolayer. The lack of the bigger debris seems to promote a smooth transition of the friction behavior for the PS400, especially during the run-in period.

As the surface gets oxidized, the contact moves directly to ceramic-ceramic contact, giving lower friction than PS304. Furthermore, since there is no stage of intense debris formation, the wear track is shallower and narrower than the PS304. Nevertheless, the delamination of the oxide layer is also observed for the PS400, and although the delamination of the oxide layer on PS304 was as blocks of oxides, for the PS400 the delamination occurs in patches along the direction of the wear track (Figure 17 (A) and (B)).

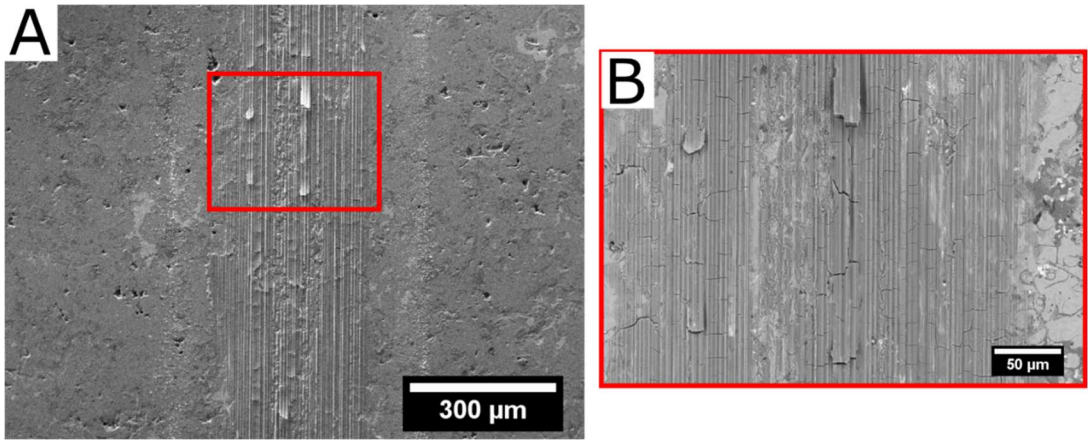

Figure 17 - Wear track of PS400 tested at room temperature after 100 hours heat treatment. (A) UVD image showing the track and the debris at the side, (B) BSE image showing oxide layer

The Raman analysis also corroborate the fact that, as wear develops on both heat-treated and not heat-treated sample, the components being formed are the same, namely silver molybdates, indicating the stability of the PS400 coating during wear and during heat treatment. Thus, the formation and presence of the molybdates on the PS400 surface seems to be key to the improved wear resistance and lower wear behavior when compared to the PS304.

4 – Conclusion

Multicomponent coatings were produced by APS and, upon heat treatments at 600°C, the formation of precipitates on the NiCr matrix of PS304 was observed, as described in literature. In the present study, EDS was used by mapping and linescan to show the composition of these precipitates: chromium fluorides formed due to the migration of fluorine from the eutectic BaF_2/CaF_2 which got oxidized forming binary and ternary oxides. These results hint that the microstructural changes occurring inside the coating are much more complex than what was originally described in literature.

For the PS400 heat treated at 600°C no precipitates were formed. Furthermore, no trace of fluorine was found in the NiAlMo matrix, indicating that the lack of direct contact between the eutectics and the matrix achieved by the layer of Al and Mo could prevent the diffusion of fluorine and prevent or at least slow the oxidation process of the eutectic mixture.

The analysis of the wear results show that it might not be possible to separate the effects of the chromium fluoride precipitates, and the effects of the oxidation of the eutectic component. The heat treatment had no clear effect on the wear behavior of PS304, and just minimal effect on the friction curves, which became more stable and the tribofilm on the surface of the coating was formed after a reduced number of cycles for the heat-treated samples. It is not clear, however, whether this was an effect of the precipitates or the oxidation of the fluorides or yet, it is not unusual for thermally sprayed coatings to have improved bonding between particles after being heat treated in this temperature range.

On the PS400, no apparent change on friction and wear was observed, which was marked by higher wear on the counterface and low wear on the coating when compared to the PS304.

The mechanism of wear of the PS304 was marked by high wear on the run-in period, with formation of wear debris up to the peak of friction. After that, a somewhat protective oxide layer, mixed with silver, was able to reduce the wear rate and to drop the fiction coefficient to levels similar to the ones found for the PS400 and in both cases, the reduced friction coefficient is attributed to the presence of ternary oxides in the wear track.

5 – Acknowledgements

The authors would like to thank the technical assistance of Dr. Fadhel Ben Ettouil with the deposition process. The authors would also like to acknowledge the financial support from Natural Sciences and Engineering Research Council (NSERC) Project Number CRDPJ 530409-18 and the Consortium for Research and Innovation in Aerospace in Québec (CRIAQ) Project Number MANU-1719 The authors would like to thank the McGill Engineering Doctoral Award (MEDA) granted to Mr. Castilho.

References

1. H. E. Sliney, "Wide temperature spectrum self-lubricating coatings prepared by plasma spray," *Thin Solid Films* **64**, 211-217 (1979).

2. P. L. Fauchais, J. V. R. Heberlein and M. I. Boulos, *Thermal Spray Fundamentals: From Powder to Part*. (Springer, 2014).

3. C. Dellacorte and J. A. Fellenstein, "The effect of compositional tailoring on the thermal expansion and tribological properties of PS300: A solid lubricant composite coating," *Tribology Transactions* **40**, 639-642 (1997).

4. C. DellaCorte and B. J. Edmonds, (NASA Center for Aerospace Information, https://ntrs.nasa.gov/citations/20090033769, 2009).

5. T. A. Blanchet, J.-H. Kim, S. J. Calabrese and C. Dellacorte, "Thrust-washer evaluation of self-lubricating PS304 composite coatings in high temperature sliding contact," *Tribology Transactions* **45**, 491-498 (2002).

6. E. E. Balic and T. A. Blanchet, "Thrust-washer tribological evaluation of PS304 coatings against Rene 41," *Wear* **259** (7), 876 (2005).

7. W. Wang, "Application of a high temperature self-lubricating composite coating on steam turbine components," *Surface & Coatings Technology* **177-178**, 12-17 (2004).

8. C. Dellacorte, "The Evaluation of a Modified Chrome Oxide Based High Temperature Solid Lubricant Coating for Foil Gas Bearings," *Tribology Transactions* **43** (2), 257-262 (2000).

9. C. Dellacorte, V. Lukaszewicz, M. J. Valco, K. C. Radil and H. Heshmat, "Performance and Durability of High Temperature Foil Air Bearings for Oil-Free Turbomachinery," *Tribology Transactions* **43** (4), 774-780 (2000).

10. C. DellaCorte, B. J. Edmonds and P. A. Benoy, "Thermal processing effects on the adhesive stregth of PS304 high temperature solid lubricant coatings," *Tribology Transactions* **45** (2002).

11. P. Ari-Gur, J. Sariel, M. K. Stanford, C. DellaCorte and P. B. Abel, "Phase identification of hard precipitates in PS304 coatings," *Surface Engineering* **27**, 196-198 (2011).

12. C. DellaCorte, "The effects of substrate material and thermal processing atmosphere on the strength of PS304: A high temperature solid lubricant coating," *Tribology Transactions* **46**, 361-368 (2003).

13. M. K. Stanford, A. M. Yanke and C. DellaCorte, *Thermal Effects on a Low Cr Modification of PS304 Solid Lubricant Coating*, 2004.

14. M. K. Stanford, "Dimensional stability, microstructure, and cohesion strength of composite solid lubricant coatings after heat treatment," *Tribology Transactions* **52**, 269-276 (2009).

15. C.-L. Ren, H. Han, W.-B. Gong, C.-B. Wang, W. Zhang, C. Cheng, P. Huai and Z.-Y. Zhu, "Adsorption and diffusion of fluorine on Cr-doped Ni(111) surface: Fluorine-induced initial corrosion of non-passivated Ni-based alloy," *Journal of Nuclear Materials* **478**, 295-302 (2016).

16. Y.-R. Yin, C.-L. Ren, H. Han, K. P. So, X.-X. Ye, X. Zhang, P. Huai and Z.-Y. Zhu, "Theoretical study of fluorine-induced surface segregation of Cr in non-passivated Ni-based alloys," *Journal of Applied Physics* **124** (13), 135302 (2018).

17. Y. R. Yin, C. L. Ren, H. Han, J. X. Dai, H. Wang, P. Huai and Z. Y. Zhu, "First-principle atomistic thermodynamic study on the early-stage corrosion of NiCr alloy under fluoride salt environment," *Physical chemistry chemical physics : PCCP* **20** (45), 28832-28839 (2018).

18. L. C. Olson, J. W. Ambrosek, K. Sridharan, M. H. Anderson and T. R. Allen, "Materials corrosion in molten LiF-NaF-KF salt," *Journal of Fluorine Chemistry* **130** (1), 67-73 (2009).

19. A. M. Aronova and G. V. Berezhkova, "Oxidation kinetics of BaF_2 single crystals," *Kristall und Technik* **14** (2), 173-178 (1979).

20. W. L. Phillips and J. E. Hanlon, "Oxygen Penetration Into Single Crystals of Calcium Fluoride," *Journal of the American Ceramic Society* **46** (9), 447-449 (1963).

21. J. H. Kim and I. S. Hwang, "Development of an in situ Raman spectroscopic system for surface oxide films on metals and alloys in high temperature water," *Nuclear Engineering and Design* **235** (9), 1029-1040 (2005).

22. M. Masoud, Y. Qiaoqin, L. Yuanshi and C.-G. Jesus, "The Effect of Deposition Parameters on the Structure and Mechanical Properties of Chromium Oxide Coatings Deposited by Reactive Magnetron Sputtering," *Coatings* **8** (3) (2018).

23. H. W. Abernathy, E. Koep, C. Compson, Z. Cheng and M. Liu, "Monitoring Ag−Cr Interactions in SOFC Cathodes Using Raman Spectroscopy," *The Journal of Physical Chemistry C* **112** (34), 13299-13303 (2008).

24. J.-H. Ouyang, X.-S. Liang, Z.-G. Liu, Z.-L. Yang and Y.-J. Wang, "Friction and wear properties of hot-pressed NiCr-BaCr2O4high temperature self-lubricating composites," *Wear* **301** (1-2), 820-827 (2013).

25. Y. W. Long, W. W. Zhang, L. X. Yang, Y. Yu, R. C. Yu, S. Ding, Y. L. Liu and C. Q. Jin, "Pressure-induced structural phase transition in CaCrO4: Evidence from Raman scattering studies," *Applied Physics Letters* **87** (18), 181901 (2005).

26. Z. Wang, S. K. Saxena, P. Lazor and H. S. C. O'Neill, "An in situ Raman spectroscopic study of pressure induced dissociation of spinel NiCr 2O 4," *Journal of Physics and Chemistry of Solids* **64** (3), 425-431 (2003).

27. J.-M. Shao, C.-W. Du, X. Zhang and L.-Y. Cui, "Effects of Lead on the Initial Corrosion Behavior of 316LN Stainless Steel in High-Temperature Alkaline Solution," *Acta Metallurgica Sinica (English Letters)* **32** (1), 89-97 (2019).

28. Z. Ma, X. Li, L. Liu and Y. Liu, "Chemical Stability between $NiCr_2O_4$ Material and Molten Calcium-Magnesium-Alumino-Silicate (CMAS) at High Temperature," *Materials (Basel, Switzerland)* **10** (12) (2017).

29. T. Zhu, C. Wang, H. Fu, W. Huang and Y. Gong, "Electrochemical and Raman Spectroscopic Investigations on the Speciation and Behavior of Chromium Ions in Fluoride Doped Molten LiCl-KCl," *Journal of The Electrochemical Society* **166** (10), H463-H467 (2019).

30. J. V. Kumar, R. Karthik, S.-M. Chen, V. Muthuraj and C. Karuppiah, "Fabrication of potato-like silver molybdate microstructures for photocatalytic degradation of chronic toxicity ciprofloxacin and highly selective electrochemical detection of H2O2," *Scientific Reports* **6** (1) (2016).

31. W. Gulbinski and T. Suszko, "Thin films of MoO3-Ag2 O binary oxides - the high temperature lubricants," *Wear* **261** (7), 867 (2006).

32. T. T. Basiev, A. A. Sobol, Y. K. Voronko and P. G. Zverev, "Spontaneous Raman spectroscopy of tungstate and molybdate crystals for Raman lasers," *Optical Materials* **15** (3), 205-216 (2000).